EPJ Appl. Metamat. 2016, **3**, 11

DOI: 10.1051/epjam/2016013

EPJ Applied Metamaterials

Available online at:
http://epjam.edp-open.org

RESEARCH ARTICLE OPEN ACCESS

Terahertz gas sensor based on absorption-induced transparency

Sergio G. Rodrigo[1,2,*]

[1] Centro Universitario de la Defensa, Carretera de Huesca, 50090 Zaragoza, Spain
[2] Instituto de Ciencia de Materiales de Aragón and Departamento de Física de la Materia Condensada, CSIC-Universidad de Zaragoza, 50009 Zaragoza, Spain

Received 7 September 2016 / Accepted 6 October 2016

Abstract – A system for the detection of spectral signatures of gases at the Terahertz regime is presented. The system consists in an initially opaque holey metal film whereby the introduction of a gas provokes the appearance of spectral features in transmission and reflection, due to the phenomenom of absorption-induced transparency (AIT). The peaks in transmission and dips in reflection observed in AIT occur close to the absorption energies of the molecules, hence its name. The presence of the gas would be thus revealed as a strong drop in reflectivity measurements at one (or several) of the gas absorption resonances. As a proof of principle, we theoretically demonstrate how the AIT-based sensor would serve to detect tiny amounts of hydrocyanic acid.

Key words: Metamaterials, Diffraction gratings, Terahertz sensing, Absorption-induced transparency.

1 Introduction

The first studies of light diffraction from apertures, patterned in metal screens, traces back to the 19th century. At first, the transmission process was believed to be severely impaired for lateral hole dimensions smaller than the wavelength of light, a view that was reinforced thanks to a theoretical prediction by Hans Bethe, reported in the mid 40's last century [1]. The prediction states that the normalized to the hole area transmission (efficiency) through a subwavelength circular hole perforating an opaque and infinitely thin metal screen, transmits a fraction T of the energy power that directly impinges onto the aperture, that at first approximation leads to $T \approx 0.24(r/\lambda)^4$, where r is the hole radius and λ the wavelength of light. For a long time this prediction along with the constraints imposed by the diffraction limit of light would result, in practice, in a lack of interest by the scientific community on light transmission through subwavelength apertures. The prediction works fine under the geometrical and material constrains above mentioned [2], while it fails for many other configurations as the discovery of extraordinary optical transmission (EOT) demonstrated [3]. The phenomenon of EOT consists in the appearance of optical resonances in the transmission spectrum of metal films drilled by subwavelength holes; featuring transmission resonances at spectral locations larger than the cutoff wavelength of the holes, with efficiencies much higher that expected by Bethe's theory, even though the finite metal thickness of real samples would additionally reduce light transmission.

Light transmission through metal foils patterned by subwavelength holes has been a very active topic of research since the discovery of EOT. Important advances in the comprehension of light diffraction by subwavelength apertures have been undertaken along the last years and different physical mechanisms involved in the EOT process were suggested and demonstrated [4–7].

The label EOT refers to a wide number of optical effects typically found in holey metal films, among other systems and type of waves [7]. Metallic films drilled by holes may feature EOT in many situations; when the holes are either isolated, randomly distributed, periodically arranged, etc. The local dielectric environment is also important [8, 9]. Depending on the value of the geometrical parameters, the number of holes and their arrangements and the presence of nearby resonant systems (like molecules), the optical transmittance may present resonances due to different mechanisms. These different physical mechanisms are responsible for [10]: surface enhanced EOT, localized EOT, absorption-induced transparency (AIT), Brewster angle EOT, and enhanced transmission through single apertures in patterned metals.

Here, we present a method for gas detection with Terahertz (THz) waves based on AIT. The AIT-based gas detector consists in a metallic hole array (HA), placed on top of a dielectric substrate (see Figure 2a) where the molecules to be detected are released in the air region, in contact with the HA (see Figure 2c). Our approach relies on the appearance of spectral features in transmission and reflection induced by the molecular specimen when this fills the holes [11],

*e-mail: sergut@unizar.es

conversely to those approaches designed to feature strong resonances at the absorption energies of the molecules [12] and, with typical functionalities based on accurately measuring spectral shifts in the presence of a given substance [13]. To illustrate our proposal we have chosen the HCN gas as the substance to be detected in the air region. Hydrogen cyanide is exhaled by motor vehicles, which is also present in tobacco in low concentrations and is extensively used in industry and manufacturing. This gas can kill a person for $\geq$300 ppm concentrations in a few minutes.

2 Absorption-induced transparency

The phenomenon of AIT was first observed in the transmission spectrum of metallic array of holes when optically active dye molecules were deposited on top of them [14]. Surprisingly, an initially opaque metallic HA may become translucent with the incorporation of the molecular compound, at the spectral range where the molecules strongly absorb electromagnetic radiation. This phenomenon results: from the excitation of surface bounded waves when the molecules form a thin layer on top of the system [15, 16]; and from the modification of the propagation constant of light inside the holes when the molecules can penetrate into them [11, 16]. Waveguide and surface AIT operate simultaneously when the dye is present both in the holes and on the surface and are found close to the absorption energy of the molecules and exist separately one each other.

Experimentally observed for electronic transitions in the visible range [14], and subsequently for molecular vibrational transitions in the infrared regime [17], it was later predicted that AIT could occur also in other frequency bands, as in the THz regime [11]. This prediction has been experimentally confirmed [18] with the use of lithium fluoride as the filling medium, a solid compound with phonon absorption bands at THz [19].

The AIT-based structure can be seen as a "metametal" which optical response can be described by means of a Drude-Lorentz model [11, 20] like in good metals. The Drude term is defined by the geometry, instead of the metal properties [21, 22], while the Lorentz term in AIT arises from each resonance of the molecules, instead of originating from interband transitions as it happens in metals. This metametal offers high flexibility for tuning either surface or wave-guide mode energies on plasmonic nanostructured arrays simply by the choice of the molecular dye.

3 AIT-based gas sensor

We have chosen for illustration one of the absorption lines of the HCN gas. Namely, the target absorption line of the HCN compound spectrally located at frequency 1239.89 GHz with a full-width at half maximum of 126 MHz [23]. The contribution to the dielectric constant of HCN from this absorption line is well represented by a Lorentz function in the frequency domain, which provides suitable optical response in the spectral window of interest for this gas, $\varepsilon_{\mathrm{HCN}}(\nu) = \varepsilon_{\mathrm{inf}} - \Delta\varepsilon\Omega^2/(\nu^2 - \Omega^2 + i\nu\Gamma)$. We obtained

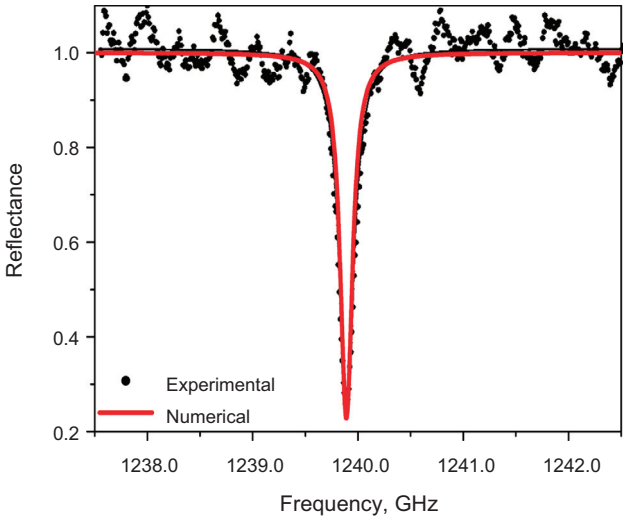

Figure 1. Transmission spectrum through a 1240 mm cell containing HCN at ≈210 ppm concentration (T = 294 K, P = 20 hPa). This absorption line corresponds to a pure rotational resonance of HCN. The experimental result (circular symbols) is extracted from Bigourd et al. [24]. The red solid line shows the analytical result using the dielectric constant for HCN described in the main text.

$\varepsilon_{\mathrm{inf}} = 1.0$, $\Delta\varepsilon = 3.5 \times 10^{-9}$, $\Gamma = 96.79$ GHz, and $\Omega = 1239.89$ GHz, which enable us to reproduce the experimental absorption spectrum obtained by Bigourd et al. [23]. The experimental sample consisted in a d = 1240 mm length cell containing HCN, at concentration of ≈210 ppm and Continuos-Wave spectroscopy was used to conduct the measurements (see Figure 1; for additional details on the experiments, see [23, 24]). Transmission was then calculated as: $T = e^{-2Im(k)d}$, where $k = \frac{2\pi}{\lambda}\sqrt{\varepsilon_{\mathrm{HCN}}}$, and from it $\varepsilon_{\mathrm{HCN}}$ was obtained.

Our theoretical analysis is based on the coupled mode method (CMM), a numerical tool which has been successfully applied to study the optical response of holey metal films [22]. The metals at THz are approximated as perfect electric conductors (PEC) in this work. The particular CMM implementation used is described in the Appendix. The advantages of using this method as compared with other numerical approaches are also discussed later on. In a few words, Maxwell's equations are solved by expanding the electromagnetic (EM) fields in the different regions of space, transmission and reflection coefficients are thus calculated by imposing appropriate boundary conditions.

The AIT-based gas detection scheme can be understood by analyzing Figure 2. Reflected THz radiation carries information about whether or not a given target substance (here hydrogen cyanide, HCN) is present inside the holes of a holey metal film. The bare holey structure must be designed to be opaque at the spectral range of interest (one of the absorption lines of the molecules). The last prerequisite can be attained in our case, for instance, perforating a thick metal film (1.0 mm) with rectangular holes (a_x = 50.0 μm, a_y = 120.9 μm) arranged in a rectangular lattice (p_x = 80.0 μm, p_y = 150.0 μm), the whole structure on top of a transparent

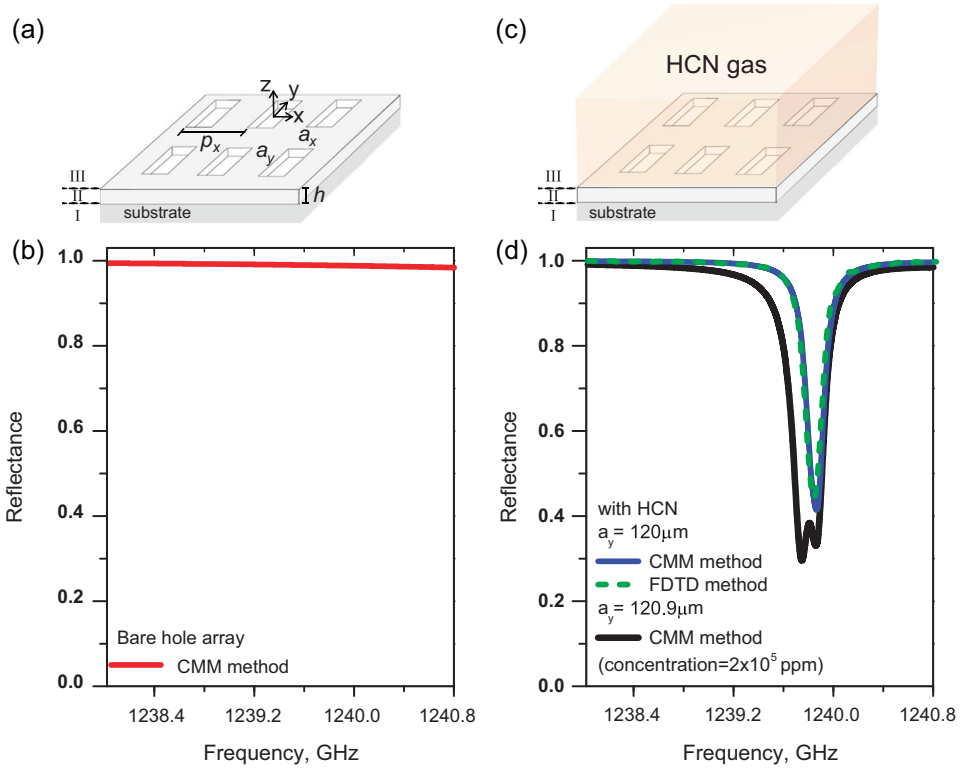

Figure 2. AIT-based gas sensor: reflected THz radiation carries information about whether or not a given target substance (here hydrogen cyanide, HCN) is present inside the holes of a holey metal film. The bare holey film (a) has been designed to be opaque at the spectral range of interest (one of the absorption lines of the molecules, Figure 1), as shown in (b). The presence of the gas (c) boosts a strong drop of reflectivity, as shown in (d). The reflection spectra were calculated with the CMM method (solid lines) and with the FDTD method (dashed line). The results for two different configurations are represented: rectangular holes with $a_x = 50.0$ μm, $a_y = 120.9$ μm (black solid line) and $a_x = 50.0$ μm, $a_y = 120.0$ μm (blue solid line and dashed line), being $\varepsilon_{III} = \varepsilon_{HCN}$ and $\varepsilon_{III} = 1$ respectively. Both HAs are arranged in a rectangular lattice ($p_x = 80.0$ μm, $p_y = 150.0$ μm) and drilled in a 1.0 mm thick metal film, everything on top of a transparent PTFE (Teflon) substrate, $\varepsilon_{PTFE} = 2.06$. The THz source is aligned so the system is illuminated at normal incidence from the substrate side (from bottom to top). The electric field points along the x-direction.

PTFE (Teflon) substrate, $\varepsilon_{PTFE} = 2.06$ [25]. The corresponding numerical result is depicted in Figure 2b. The presence of the gas (Figure 2c) boosts a strong drop of reflectivity for the HCN concentration chosen (black solid line, Figure 2d).

The performance of the AIT-based detector in terms of HCN concentration is shown in Figure 3a. In this figure the reflection contrast, defined as: $\Delta R = R_{HA} - R_{HA+HCN} \approx 1 - R_{HA+HCN}$, is represented as a function of frequency for different HCN molecular concentrations. In the main panel, the maximum value of ΔR is shown as a function of the density of HCN in the system. In order to exploit the AIT configuration at fixed wavelength and low concentrations, a potential experimental setup should incorporate high sensitivity and spectral resolution detectors, able to discriminate small changes on reflectance at fixed wavelengths. A contrast value of $\Delta R_{max} \approx 10^{-4}$ would be necessary to detect at the 9 ppm level, which for HCN has been considered competitive for THz spectroscopy as compared to chemical analytical methods [24].

We have checked that the device performance is not impaired even if the film thickness, periodicity and short side of the rectangles are changed by several microns. Figure 3b shows the reflectance calculated as a function of the film thickness (from 0.5 mm to 2.0 mm) for the period and hole dimensions of Figure 2. The long side of the rectangles would require more precise tuning during the fabrication process, with a tolerance range of approximately ±500 nm, as it is shown in the calculations of reflectance for the bare structure and when the HCN gas is present, Figures 3c and 3d respectively. The AIT-based gas sensor, which action requires both a bare structure with high reflectivity and spectral selectivity once the gas is introduced (only one spectral feature close to the target absorption line, with similar spectral bandwidth), does not work fine for $a_y > 121.5$ μm, as shown in Figures 3c–3d. That accuracy is however perfectly available with current nanofabrication techniques [26] that allowed to produce gaps as small as 2 nm in micro sized structures [27].

The AIT configuration could operate in transmission or reflection mode (or both) depending on the setup conditions. The gas must fill the holes in both cases, at least partially, for a good performance of the sensor [11]. Definitely, the output region should not contain gas in transmission mode. We have checked that reflectance does not change appreciably if HCN is removed from the transmission region as compared to the situation where the gas is released everywhere, at least for the geometrical parameters investigated here. Note however

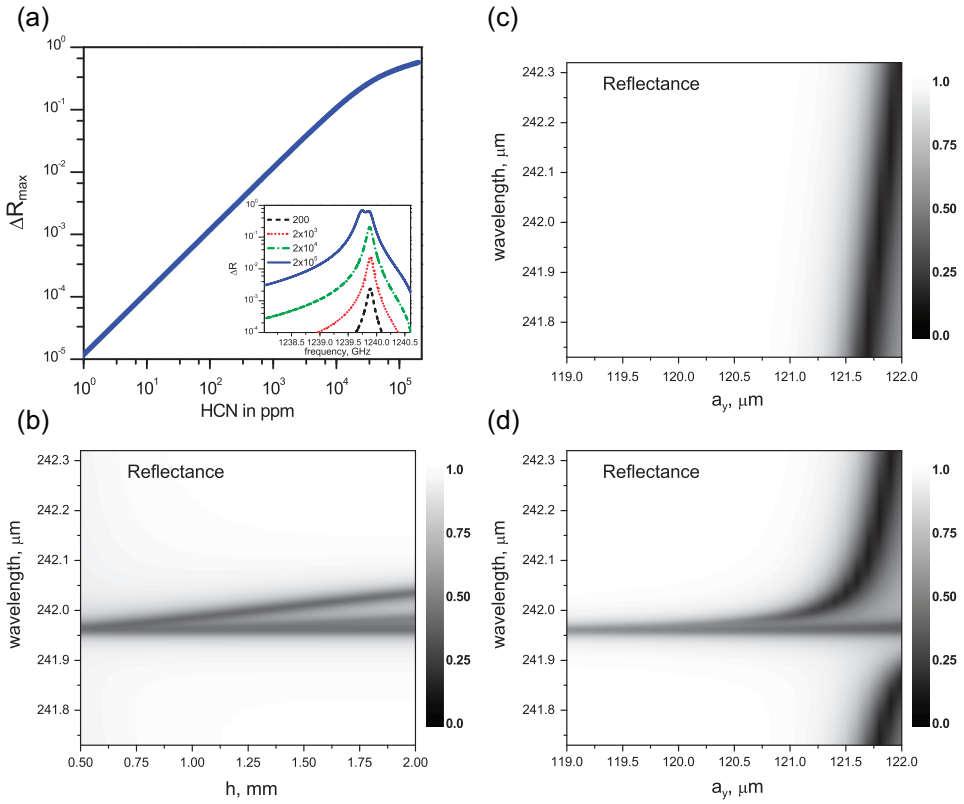

Figure 3. (a) Reflection contrast, ΔR, as a function of the amount of HCN within the holes (in ppm) at the spectral locations of ΔR, maxima. Inset: ΔR, as function of the frequency for different HCN concentrations. Reflectance as function of (b) the film thickness and (c)–(d) the long side of the rectangles. In (b) and (d) the HCN concentration is 2×10^5 ppm, while in (c) the system is free of gas (bare structure). The geometry of (a) and (b) is similar that of Figure 2, where $a_y = 120.9$ μm. In (c) and (d) $h = 1$ mm. In all cases $\varepsilon_{III} = \varepsilon_{HCN}$.

that this would not be the case if multiple scattering can not be neglected. In fact, the appearance of the double dip is related with the building up process of reflectance. When multiple reflections of light (going back and forth inside the holes) can be neglected, transmission can be described as a non-resonant three steps process and only one dip in reflection is seen [11]. In that case the reflectance depends only on the Fresnel's coefficients of the I–II interface (surface of illumination). The reflection mode has an additional advantage, the dielectric substrate acts as a shield to prevent HCN leakage from the transmission region to the reflection region, which are thus isolated from each other. In that case, both detector and source could be safely located at the same side, with the molecules dispersed in the transmission zone (a reaction chamber, for instance).

Finally, we discuss the advantages of the CMM method as compared to other widely used numerical methods. We have compared the results obtained with CMM with those obtained with the finite-difference time-domain (FDTD) method [28]. To compute the scattering coefficients with FDTD, the different diffracted orders can be obtained by projecting onto diffracted modes in each dielectric half-space. The basic idea consists in finding a way to isolate the current that each wave-vector of the reciprocal lattice carries, as a function of both the wavelength and the polarization state (for further details see [29, 30] and references therein). The PEC approximation is achieved by forcing the parallel components of the electric field on the metal surfaces to be zero. The linear response of HCN is described by a Lorentz function [31, 32]. The infinite periodic hole array is numerically cast into a finite system applying Bloch's condition at the boundaries of the unit cell (x- and y-directions) and imposing "uniaxial perfect matched layers" at surfaces parallel to the metal film through the z-direction. Our computational resources (computer memory and clock speed) constrained the FDTD simulations to systems with mesh size not much smaller than 2.5 μm. We could not choose for instance $a_y = 120.9$ μm, so to compare identical structures with both methods a different value was chosen, $a_y = 120.0$ μm. We faced an additional problem: complex values of the dielectric constant of the superstrate are not supported by our FDTD program, so $\varepsilon_{III} = 1$ is taken for the sake of comparison. The FDTD result, shown with a dashed line in Figure 2d, converged after several days, whereas the CMM calculation (blue solid line, same figure) took just a few seconds to finish.

4 Conclusions

A detection method has been presented based on AIT, exemplarily able to recognize the presence of the poisonous HCN gas. Our method is neither constrained to a specific chemical compound nor to the geometrical parameters used.

As a component of a sensing device, the AIT configuration would provide field enhancement, introducing further advantages over bulk THz spectroscopy, like chemical functionalization for molecular trapping. The patterning of different holes (periodically arranged or not) with different shapes and sizes on the same sample, each one designed for covering one of several characteristic wavelengths of a single molecular compound (or a mixture of them) might lead to multispectral detection based on AIT. Therefore, the AIT configuration might become a complementary method to existing ones for applications in sensing at THz [13].

More speculative, AIT-based systems could be exploited in THz field-matter interaction research led by recent advances in intense THz sources [33, 34]. Strong light-matter interactions can take place through intense THz fields. A THz beam can provoke crystal lattice or electron excitations, molecular rotation or charge acceleration, among others. The optical response of an AIT-based device would be affected by any of these mechanisms if the intense THz fields induced changes on the refractive index inside the holes. In the case AIT was induced by the presence of a gas, gas ionization could change the optical response. In crystalline solids supporting phonon modes, high THz fields would provide access to anharmonic parts of the interaction potential that also would change the AIT response. The phenomenon of AIT has been associated to electronic transitions in the visible range, molecular vibrational transitions in the infrared, and rotational transitions in the THz range. In general, AIT could be found in any spectral region whenever the material optical response has a well defined absorption resonance. Therefore the nonlinear response of different materials would affect AIT in very unexpected ways, we hope some of them interesting.

Acknowledgements. We acknowledge support from the Spanish Ministry of Economy and Competitiveness under project MAT2014-53432-C5-1-R.

References

1. H.A. Bethe, Theory of diffraction by small holes, Phys. Rev. 66 (1944) 163.
2. A.Yu. Nikitin, D. Zueco, F.J. García-Vidal, L. Martín-Moreno, Electromagnetic wave transmission through a small hole in a perfect electric conductor of finite thickness, Phys. Rev. B 78 (2008) 165429.
3. T.W. Ebbesen, H.L. Lezec, H.F. Ghaemi, T. Thio, P.A. Wolff, Extraordinary optical transmission through subwavelength hole arrays, Nature 391 (1998) 667–669.
4. C. Genet, T.W. Ebbesen, Light in tiny holes, Nature 445 (2007) 39–46.
5. F.J. García de Abajo, Colloquium: light scattering by particle and hole arrays, Rev. Mod. Phys. 79 (2007) 1267.
6. R. Gordon, A.G. Brolo, D. Sinton, K.L. Kavanagh, Resonant optical transmission through hole-arrays in metal films: physics and applications, Laser Photon. Rev. 4 (2009) 311–335.
7. F.J. Garcia-Vidal, L. Martin-Moreno, T.W. Ebbesen, L. Kuipers, Light passing through subwavelength apertures, Rev. Mod. Phys. 82 (2010) 729–787.
8. A. Krishnan, T. Thio, T.J. Kim, H.L. Lezec, T.W. Ebbesen, P.A. Wolff, J.B. Pendry, L. Martín-Moreno, F.J. García-Vidal, Evanescently coupled resonance in surface plasmon enhanced transmission, Opt. Commun. 200 (2001) 1–7.
9. S. Carretero-Palacios, F.J. García-Vidal, L. Martín-Moreno, S.G. Rodrigo, Effect of film thickness and dielectric environment on optical transmission through subwavelength holes, Phys. Rev. B 85 (2012) 035417.
10. S.G. Rodrigo, F. de León-Pérez, L. Martín-Moreno, Extraordinary optical transmission: fundamentals and applications, Proc. IEEE (2016). DOI: 10.1109/JPROC.2016.2580664.
11. S.G. Rodrigo, F.J. García-Vidal, L. Martín-Moreno, Theory of absorption-induced transparency, Phys. Rev. B 88 (2013) 155126.
12. H.-R. Park, K.J. Ahn, S. Han, Y.-M. Bahk, N. Park, D.-S. Kim, Colossal absorption of molecules inside single terahertz nanoantennas, Nano Lett. 13 (2013) 1782–1786.
13. J.F. O'Hara, W. Withayachumnankul, I. Al-Naib, A review on thin-film sensing with terahertz waves, J. Infrared. Millim. TE 33 (2012) 245–291.
14. J.A. Hutchison, D.M. O'Carroll, T. Schwartz, C. Genet, T.W. Ebbesen, Absorption-induced transparency, Angew. Chem. Int. Ed. 50 (2011) 2085–2089.
15. W.-H. Yeh, J.W. Petefish, A.C. Hillier, Resonance quenching and guided modes arising from the coupling of surface plasmons with a molecular resonance, Anal. Chem. 84 (2012) 1139–1145.
16. X. Zhong, S.G. Rodrigo, L. Zhang, P. Samori, C. Genet, L. Martin-Moreno, J.A. Hutchison, T.W. Ebbesen, Waveguide and plasmonic absorption-induced transparency, ACS Nano 10 (2016) 4570–4578.
17. E.J. Osley, C.G. Biris, P.G. Thompson, R.R.F. Jahromi, P.A. Warburton, N.C. Panoiu, Fano resonance resulting from a tunable interaction between molecular vibrational modes and a double continuum of a plasmonic metamolecule, Phys. Rev. Lett. 110 (2013) 087402.
18. M.F. Acosta, S.G. Rodrigo, L. Martín-Moreno, C. Pecharromán, R.I. Merino, Micropillar templates for dielectric filled metal arrays and flexible metamaterials, Adv. Opt. Mater. (2016). DOI: 10.1002/adom.201600670.
19. R.I. Merino, M.F. Acosta, V.M. Orera, New polaritonic materials in the THz range made of directionally solidified halide eutectics, J. Eur. Ceram. Soc. 34 (2014) 2061–2069.
20. S.G. Rodrigo, L. Martín-Moreno, Absorption-induced transparency metamaterials in the terahertz regime, Opt. Lett. 41 (2016) 293–296.
21. J.B. Pendry, L. Martín-Moreno, F.J. García-Vidal, Mimicking surface plasmons with structured surfaces, Science 305 (2004) 847–848.
22. L. Martín-Moreno, F.J. García-Vidal, Minimal model for optical transmission through holey metal films, J. Phys.: Condens. Matter 20 (2008) 304214.
23. D. Bigourd, A. Cuisset, F. Hindle, S. Matton, E. Fertein, R. Bocquet, G. Mouret, Detection and quantification of multiple molecular species in mainstream cigarette smoke by continuous-wave terahertz spectroscopy, Opt. Lett. 31 (2006) 2356–2358.
24. D. Bigourd, A. Cuisset, F. Hindle, S. Matton, R. Bocquet, G. Mouret, F. Cazier, D. Dewaele, H. Nouali, Multiple component analysis of cigarette smoke using THz spectroscopy, comparison with standard chemical analytical methods, Appl. Phys. B 86 (2007) 579–586.

25. J.A. Hejase, P.R. Paladhi, P. Chahal, Terahertz characterization of dielectric substrates for component design and nondestructive evaluation of packages, IEEE Trans. Compon. Packag. Manuf. Technol. 1 (2011) 1685–1694.
26. X. Chen, H.-R. Park, M. Pelton, X. Piao, N.C. Lindquist, H. Im, Y.J. Kim, J.S. Ahn, K.J. Ahn, N. Park, D.-S. Kim, S.-H. Oh, Atomic layer lithography of wafer-scale nanogap arrays for extreme confinement of electromagnetic waves, Nature Commun. 4 (2013) 2361.
27. H.-R. Park, S. Namgung, X. Chen, S.-H. Oh, High-density metallic nanogap arrays for the sensitive detection of single-walled carbon nanotube thin films, Faraday Discuss. 178 (2015) 195–201.
28. A. Taove, S.C. Hagness, Computational electrodynamics: the finite-difference timedomain method. 3rd ed., Artech House, Boston, 2005.
29. S.G. Rodrigo, F.J. García-Vidal, L. Martín-Moreno, Influence of material properties on extraordinary optical transmission through hole arrays, Phys. Rev. B 77 (2008) 075401.
30. S.G. Rodrigo, Optical properties of nanostructured metallic systems: studied with the finite-difference time-domain method, Springer Theses, Springer, 2011.
31. R.J. Luebbers, F. Hunsberger, FDTD for Nth-order dispersive media, IEEE Trans. Antennas Propag. 40 (1992) 1297.
32. F. Hao, P. Nordlander, Efficient dielectric function for FDTD simulation of the optical properties of silver and gold nanoparticles, Chem. Phys. Lett. 446 (2007) 115–118.
33. J. Gu, R. Singh, X. Liu, X. Zhang, Y. Ma, S. Zhang, S.A. Maier, Z. Tian, A.K. Azad, H.-T. Chen, A.J. Taylor, J. Han, W. Zhang, Active control of electromagnetically induced transparency analogue in terahertz metamaterials, Nature Commun. 3 (2012) 1151.
34. T. Kampfrath, K. Tanaka, K.A. Nelson, Resonant and nonresonant control over matter and light by intense terahertz transients, Nature Photon. 7 (2013) 680–690.
35. A. Roberts, R.C. McPhedran, Bandpass grids with annular apertures, IEEE Trans. Antennas Propag. 36 (1988) 607–611.
36. F. de Leon-Perez, G. Brucoli, F.J. Garcia-Vidal, L. Martin-Moreno, Theory on the scattering of light and surface plasmon polaritons by arrays of holes and dimples in a metal film, New J. Phys. 10 (2008) 105017.
37. J. Bravo-Abad, F.J. García-Vidal, L. Martín-Moreno, Resonant transmission of light through finite chains of subwavelength holes in a metallic film, Phys. Rev. Lett. 93 (2004) 227401.
38. F.J. García-Vidal, E. Moreno, J.A. Porto, L. Martín-Moreno, Transmission of light through a single rectangular hole, Phys. Rev. Lett. 95 (2005) 103901.
39. F. Lopez-Tejeira, S.G. Rodrigo, L. Martin-Moreno, F.J. Garcia-Vidal, E. Devaux, J. Dintinger, T.W. Ebbesen, J.R. Krenn, I.P. Radko, S.I. Bozhevolnyi, M.U. Gonzalez, J.C. Weeber, A. Dereux, Modulation of surface plasmon coupling-in by one-dimensional surface corrugation, New J. Phys. 10 (2008) 033035.
40. A.I. Fernández-Domínguez, I. Hernández-Carrasco, L. Martín-Moreno, F.J. García-Vidal, Transmission resonances through a Fibonacci array of subwavelength slits, Electromagnetics 28 (2008) 186–197.
41. C.R. Williams, M. Misra, S.R. Andrews, S.A. Maier, S. Carretero-Palacios, S.G. Rodrigo, F.J. García-Vidal, L. Martín-Moreno, Dual band terahertz waveguiding on a planar metal surface patterned with annular holes, Appl. Phys. Lett. 96 (2010) 011101.

Cite this article as: Rodrigo SG: Terahertz gas sensor based on absorption-induced transparency. EPJ Appl. Metamat. 2016, **3**, 11.

Appendix: Coupled Mode Method

The CMM method provides fast and accurate results as compared to other numerical models widely used in computational electromagnetism.

Next, the CMM implementation used in this work, applied to perfectly conducting HAs, is briefly discribed [22]. As already explained, Maxwell's equations are solved by expanding the EM fields in the different regions of space, transmission and reflection coefficients are thus calculated by imposing appropriate boundary conditions [7]. The metal is chosen to be a PEC ($|\varepsilon_{\text{metal}}| = \infty$), which is a good approximation in the THz regime for geometrical features much larger than the skin depth. The whole space is divided in three regions (see Figure 2a): (I) the substrate, (II) holes and, (III) the superstrate.

In region (II) the EM field is expanded in terms of TE and TM waveguide eigenmodes. However, good convergence is attained only by considering the less decaying transversal electric mode, $TE_{0,1}$ for subwavelength rectangular holes (the fundamental waveguide mode). Within this "minimal model", results can be worked out analytically [9]. The in-plane electric field component of the $TE_{0,1}$ mode is defined as:

$$\vec{E}_{||}^{\text{TE}}(\vec{r}_{||}) = \sqrt{\frac{2}{a_x a_y}}\left(\sin[q_y(y + a_y/2)], 0\right) \tag{A.1}$$

within the interval $\vec{r}_{||} \in [-a_y/2, a_y/2] \times [-a_x/2, a_x/2]$ and zero otherwise, where $q_y = \pi/a_y$ is the only component of its parallel wave-vector, being the corresponding propagation constant $q_z = \sqrt{\varepsilon_{\text{II}} g^2 - q_y^2}$, with $g = 2\pi/\lambda(\varepsilon_{\text{II}} = \varepsilon_{\text{hole}})$.

In the substrate ($\varepsilon_{\text{I}} = \varepsilon_{\text{substrate}}$) and the superstrate ($\varepsilon_{\text{III}} = \varepsilon_{\text{superstrate}}$) the EM fields are expressed in terms of plane waves, characterized by the in-plane component of the wave-vector $\vec{k}_{||} = (k_x, k_y)$ and, satisfying the z-component the isotropic dispersion relation $k_z = \sqrt{\varepsilon_{\text{I,III}} g^2 - k_{||}^2}, k_{||}^2 = k_x^2 + k_y^2$.

By matching the EM fields at the interfaces, we end up with a set of two coupled linear equations where the electric field amplitude of the fundamental mode at the input side, E, $[\vec{e}(z = -h) = E\,\vec{E}_{||}^{TE}(r_{||})]$, and at the output side, E', $[\vec{e'}(z = 0) = -E'\vec{E}_{||}^{TE}(r_{||})]$, are unknowns:

$$\begin{aligned} (G^{\text{I}} - \Sigma)\,E - G_v\,E' &= I_0 \\ (G^{\text{III}} - \Sigma)\,E' - G_v\,E &= 0 \end{aligned} \tag{A.2}$$

Equations (A.2) lead to the solution:

$$\begin{aligned} E &= \frac{I_0(G^{\text{III}} - \Sigma)}{(G^+ - \Sigma)^2 - G_v^2 - (G^-)^2} \\ E' &= \frac{I_0 G_v}{(G^+ - \Sigma)^2 - G_v^2 - (G^-)^2} \end{aligned} \tag{A.3}$$

here $G^{\pm} = [G^{\text{I}}(\lambda, \varepsilon_{\text{I}}) \pm G^{\text{III}}(\lambda, \varepsilon_{\text{III}})]/2$.

The different terms in these equations have a simple physical interpretation. The EM coupling between the input and the output side of the holes to the continuum of plane waves is mediated by the Green's functions $G^{\text{I}}(\lambda, \varepsilon_{\text{I}})$ and $G^{\text{III}}(\lambda, \varepsilon_{\text{III}})$, respectively. The general expression for these functions can be expressed as $G^{\text{I}} = i\sum_{\vec{k}\,\sigma} Y^{\text{I}}_{\vec{k}\,\sigma} |S_{\vec{k},\sigma}|^2$, where σ stands for the polarization ($\sigma = p$ or $\sigma = s$). Here, $Y^{\text{I}}_{\vec{k}\,s} = k_z/g$ and $Y^{\text{I}}_{\vec{k}\,p} = \varepsilon_{\text{I}} g/k_z$ (and the same for G^{III} with ε_{III}). Note that the $\vec{k}$-vector runs over the reciprocal lattice vectors, that is, for a rectangular lattice $k_x = \frac{2\pi}{p_x} n$ and $k_y = \frac{2\pi}{p_y} m$ (n and m being integer numbers). Usually a few difracction orders are enough to obtain converged results. On the other hand, the coupling between the fundamental mode and free-space modes comes from overlap integrals which depend upon the specific hole shape [35, 36], in our case:

$$S_{\vec{k},\sigma} = \int dr_{||}\,\vec{V}_\sigma \cdot \vec{E}_{||}^{\text{TE}}(r_{||})\,\frac{e^{i\vec{k}_{||}\cdot\vec{r}_{||}}}{\sqrt{p_x p_y}} \tag{A.4}$$

where $\vec{V}_p = (k_x, k_y)/k_{||}$ and $\vec{V}_s = (-k_y, k_x)/k_{||}$ for $k_{||} \neq 0$. For for $k_{||} = 0$, $\vec{V}_p = (1, 0)$ and $\vec{V}_s = (0, 1)$, so for rectangular holes:

$$S_{\vec{k},\sigma} = \frac{\sqrt{a_x a_y}}{\sqrt{2p_x p_y}}\,f_{\vec{k},\sigma}\text{sinc}[k_x a_x/2] \cdot \left(\text{sinc}\left[\frac{(k_y + q_y)a_y}{2}\right] + \text{sinc}\left[\frac{(k_y - q_y)a_y}{2}\right]\right) \tag{A.5}$$

where $\text{sinc}[x] = \sin[x]/x$ and $f_{\vec{k},p} = k_x/k_{||}$, $f_{\vec{k},s} = -k_y/k_{||}$, for $k_{||} \neq 0$. For $k_{||} = 0$, $f_{\vec{k},p} = 1$ and $f_{\vec{k},s} = 0$.

The real part of these Green's functions (G_r) controls the matching between the fundamental waveguide mode and the evanescent EM modes in vacuum, and so does the imaginary part (G_i) with the propagating modes.

The term I_0 measures the overlap between the incident plane wave and the fundamental mode inside the hole:

$$I_0 = 2i\,Y^{I}_{\vec{k}_0,\sigma_0} S_{\vec{k}_0,\sigma_0} \tag{A.6}$$

The term G_v controls the EM coupling between the input and the output sides of the holes:

$$G_v = 2i\,\frac{q_z}{g}\,\frac{e^{iq_z h}}{e^{2iq_z h} - 1} \tag{A.7}$$

Finally, the expression for Σ is given by:

$$\Sigma = i\,\frac{q_z}{g}\,\frac{e^{2iq_z h} + 1}{e^{2iq_z h} - 1} \tag{A.8}$$

To obtain the transmittance T at normal incidence, within the minimal model approximations, we have to impose $\vec{k}_0 = (0,0)$ and $\sigma = p$. Transmittance finally reads:

$$T = G_i^{\mathrm{III}} |E'|^2 / \sqrt{\varepsilon_{\mathrm{I}}} \tag{A.9}$$

and reflectance:

$$R = 1 - 2Re\left[S_{\vec{k}_0,\sigma_0} E\right] + G_i^{\mathrm{I}} |E|^2 / \sqrt{\varepsilon_{\mathrm{I}}} \tag{A.10}$$

AIT is not restricted to rectangular hole arrays operating in the THz regime [16]. The CMM method can be applied to more complex structures (holes, annular holes, grooves, slits, etc.) where the real properties of metals can be taken into account and including additional EM modes inside the apertures [2, 7, 36–41].